FOLIA HISTOCHEMICA ET CYTOBIOLOGICA
Vol. 62, No. 1, 2024
pp. 37–49

ORIGINAL PAPER

VIA MEDICA

Immunocytochemical localization of nitric oxide synthase-containing neurons in the visual cortex of the Mongolian gerbil

Xin-Yu Kuai*, Gwang-Jin Jeong*, Chang-Jin Jeon

Department of Biology, School of Life Sciences, BK21 FOUR KNU Creative BioResearch Group, College of Natural Sciences, and Brain Science and Engineering Institute, and Research Institute for Dok-do and Ulleung-do Island, Kyungpook National University, Daegu, Korea

*Both authors contributed equally to this work.

Abstract

Introduction. Nitric oxide (NO) is present in various cell types in the central nervous system and plays a crucial role in the control of various cellular functions. The diurnal Mongolian gerbil is a member of the rodent family Muridae that exhibits unique physiological, anatomical, and behavioral differences from the nocturnal rat and mouse, which render it a useful model for studying the visual system. The purpose of this study was to confirm the distribution and morphology of neurons that contain nitric oxide synthase (NOS) and their pattern of co-expressing NOS with neuropeptide Y (NPY), somatostatin (SST), and gamma-aminobutyric acid (GABA) in the visual cortex of Mongolian gerbils.

Materials and methods. Mongolian gerbils were used in the study. We confirmed the localization of NOS in the visual cortex of Mongolian gerbils using horseradish peroxidase immunocytochemistry, fluorescent immunocytochemistry, and conventional confocal microscopy.

Results. NOS-immunoreactive (IR) neurons were present in all layers of the visual cortex of the Mongolian gerbil, with the exception of layer I, with the highest density observed in layer V (50.00%). The predominant type of NOS-IR neurons was multipolar round/oval cells (60.96%). Two-color immunofluorescence revealed that 100% NOS-IR neurons were co-labeled with NPY and SST and 34.55% were co-labeled with GABA.

Conclusions. Our findings of the laminar distribution and morphological characteristics of NOS-IR neurons, as well as the colocalization patterns of NOS-IR neurons with NPY, SST, and GABA, indicated the presence of species-specific differences, suggesting the functional diversity of NO in the visual cortex. This study provides valuable data on the anatomical organization of NOS-IR neurons and, consequently, a better understanding of the functional aspects of NO and species diversity. *(Folia Histochemica et Cytobiologica 2024, Vol. 62, No. 1, 37–49)*

Keywords: Mongolian gerbil; visual cortex; nitric oxide synthase; neuropeptide Y; somatostatin; gamma-aminobutyric acid; immunocytochemistry

Introduction

Nitric oxide (NO) plays a crucial role in governing diverse cellular functions, and is recognized as a key influencer and mediator of many physiological processes, such as the regulation of synaptic transmission [1–4], vasodilation [5], the facilitation of neural development [4, 5], antioxidant activity [5, 6], immune modulation [5, 7], enhancement of learning and memory [7–9], and the modulation of neuronal survival [4, 6, 7]. NO is produced intracellularly by the neuronal nitric oxide synthase (nNOS) and serves as a neurotransmitter within the central nervous system (CNS) [4, 7, 10]. NOS-containing neurons have been localized in the visual cortex of many animals including human

Correspondence address:
Prof. Chang-Jin Jeon
Neuroscience Lab., Department of Biology,
College of Natural Sciences,
Kyungpook National University, 80, Daehak-ro, Daegu,
41566, South Korea
phone: +82-53-950-5343, fax: +82-53-953-3066,
e-mail: cjjeon@knu.ac.kr

Folia Histochem Cytobiol. 2024
DOI: 10.5603/fhc.99227
ISSN 0239-8508, e-ISSN 1897-5631

[11], monkey [12, 13], rabbit [14], hamster [15], rat [16–18], bat [19], and mouse [14]. NOS-containing neurons are distributed through layers I–VI of visual cortex in monkeys [12], rabbits [14], hamsters [15], bats [19], and mice [14], whereas in the visual cortex of humans [11], and rats [18], the NOS-containing neurons are absent in layer I and distributed through layer II–VI.

Neuropeptide Y (NPY) is one of the most highly expressed neuropeptides across the central and peripheral nervous systems of mammals [20–23]. NPY-containing neurons are distributed in layers II–VI of the gerbil visual cortex and include at least six morphologically different cell types [24]. Somatostatin (SST) exhibits widespread expression throughout the brain and plays diverse significant roles [25–31]. SST-containing neurons are distributed in layers II–VI of the gerbil visual cortex and include four morphologically different cell types [32]. Gamma-aminobutyric acid (GABA) serves as the primary inhibitory neurotransmitter in the CNS and plays a crucial role in the regulation of the balance between excitation and inhibition among neurons [33–35]. This balance is critically important for the processing and filtering of visual information, thus contributing to the maintenance of the normal function of the visual system [36]. The colocalization of NOS in the neurons of the cerebral cortex, including the visual cortex, with various chemical markers, such as NPY [37], SST [16, 37], and GABA [16, 38, 39] indicates that NOS-containing neurons can be divided into subtypes based on the patterns of co-expression of NOS with NPY, SST, and GABA.

The Mongolian gerbil (*Meriones unguiculatus*) is a small mammal of the rodent Muridae family that has become a suitable laboratory model species [40]. As such, gerbils have been extensively used in the fields of aging [41–43], metabolism [44–46], infection [47, 48], immune system [49, 50], and cancer [51, 52]. In neuroscience research, gerbils have been extensively used to study sensory systems [53–58], neurological diseases [54, 59–61] and brain structures [62–64]. Gerbils have benefits especially in visual studies, because gerbils are physiologically, anatomically, and behaviorally different from rats and mice, although they belong to the same family [65–68]. For example, both rats and mice are nocturnal animals with rod-dominated retinas [67, 68], whereas gerbils are diurnal animals with a higher proportion of retinal cones [67–69], which results in a higher visual acuity compared with that of rats and mice [70]. In addition, gerbils have a specialized retinal area that is similar to the central fovea in humans, which does not exist in rats and mice [67, 71]. These characteristics support the use of gerbils instead of rats and mice in comparative studies related to vision. Therefore, gerbils have been used in studies of central visual systems, such as the retina [67, 68, 72, 73], and the visual cortex [53–55, 74].

The distribution and morphology of NOS-containing neurons have not been studied in the gerbil visual cortex. Therefore, in this study, we investigated the organization of NOS-containing neurons using commercially available specific antibodies for nNOS. Firstly, we examined the laminar distribution and morphology of NOS-immunoreactive (IR) neurons using immunocytochemistry, quantitative analysis, and conventional/confocal microscopy, to determine whether NOS-IR neurons are present in specific layers and morphological types in the gerbil visual cortex. Secondly, we examined the colocalization pattern of NOS with NPY, SST, and GABA in the gerbil visual cortex, to determine whether NOS-IR neurons are a subpopulation of NPY-, SST-, or GABA-IR neurons. Thirdly, we compared the laminar distribution and morphology of NOS-IR neurons, as well as the differences in colocalization with NPY, SST, and GABA, with those of other previously studied species, to determine the presence/absence of species similarities and differences. Finally, these results will provide valuable information toward the understanding of NOS-IR neurons, the species-specific expression of NOS, and species diversity.

Materials and methods

Animals and tissue preparation. Ten Mongolian gerbils (*Meriones unguiculatus*) (22–24 months of age; weight, 110–130 g) obtained from a local supplier were used in this study. After anesthesia *via* isoflurane inhalation (1.5% dissolved in 70% nitrous oxide), the animals were perfused intracardially with 4% paraformaldehyde and 0.3–0.5% glutaraldehyde in 0.1 M sodium phosphate buffer (pH 7.4) containing 0.002% calcium chloride. After pre-washing with approximately 60 mL of 0.1 M phosphate-buffered saline (PBS; pH 7.4) for 5 minutes, 75 mL of fixative was instilled into each gerbil for 6 minutes through a syringe needle that was inserted into the left ventricle and aorta of the animal. The animals were decapitated, and the brains were gently removed from the skulls, placed in fixative overnight, then mounted on chucks and sliced into 50-μm-thick coronal sections using a Vibratome 3000 Plus Slicing System (Vibratome, St. Louis, MO, USA). All animal experiments were approved by the committee of Kyungpook National University (permission NO. 2023-0317). Guide for the Care and Use of Laboratory Animals (https://grants.nih.gov/grants/olaw/guide-for-the-care-and-use-of-laboratory-animals.pdf) were followed.

Horseradish peroxidase staining. A monoclonal mouse anti-NOS antibody (diluted at 1:200 in PBS; BD Biosciences, San Jose, CA, USA) was used as the primary antibody. Standard

Folia Histochem Cytobiol. 2024
DOI: 10.5603/fhc.99227
ISSN 0239-8508, e-ISSN 1897-5631

immunocytochemical techniques and methods were used in this experiment, as described previously [75]. Briefly, the tissues were incubated in 1% sodium borohydride (Sigma-Aldrich, Saint Louis, MO, USA) for 30 min. Afterward, the tissues were rinsed for 3 × 10 min in 0.1M PBS, then incubated in PBS with 4% normal horse serum (Vector Laboratories, Burlingame, CA, USA) with 0.5% Triton X-100 for 2 h. Next, the tissues were incubated for 2 overnights with primary antibody. After rinsed with PBS, the tissues were incubated in a 1:140 dilution of biotinylated secondary horse anti-mouse IgG (Vector Laboratories) for 2 h and rinsed with PBS. Afterward, the tissues were incubated in the avidin-biotinylated horseradish peroxidase complex (diluted at 1:50; Vector Laboratories,) for 2 h. The tissues were rinsed in 0.25 M Tris buffer for 3 × 10 min. Finally, staining was visualized by reacting with 1,3'-diaminobenzidine tetrahydrochloride (DAB) and hydrogen peroxide in 0.25 M Tris buffer for 30–60 seconds, using a DAB reagent kit (Seracare, Milford, MA, USA). The tissues were then rinsed in 0.25 M Tris buffer, mounted on Superfrost Plus slides (Fisher, Pittsburgh, PA, USA) and dried overnight in a 37°C oven. The mounted sections were dehydrated with ethanol, cleared with xylene, and then coverslips were applied with Permount (Fisher). Labeled sections were examined and photographed using a Zeiss Axioplan microscope (Carl Zeiss Meditec, Jena, Germany) with conventional or differential interference contrast (DIC) optics.

Fluorescence immunocytochemistry. For the double labeling of NOS with NPY, SST, or GABA, standard immunocytochemical methods were used, as described previously [75]. The primary antibodies used here were as follows: mouse anti-NOS (BD Biosciences), rabbit anti-NPY (Immunostar, Hudson, WI, USA), rat anti-SST (Millipore Corporation, Temecula, CA, USA), rabbit anti-GABA (Sigma-Aldrich), and guinea pig anti-GABA (Sigma-Aldrich). The primary antibodies were diluted at 1:500 (NOS, NPY, SST) or 1:200 (GABA). The secondary antibodies used here were as follows: Cy3-conjugated anti-mouse IgG (Jackson ImmunoResearch, Baltimore, PA, USA) or fluorescein (FITC)-conjugated anti-mouse IgG (Vector Laboratories, Burlingame, CA, USA) to detect NOS; Cy3-conjugated anti-rabbit IgG (Jackson ImmunoResearch) to detect NPY; Cy3-conjugated anti-rat IgG (Jackson ImmunoResearch) to detect SST; and FITC-conjugated anti-guinea pig (Jackson ImmunoResearch) or Cy3-conjugated anti-rabbit IgG (Sigma-Aldrich) to detect GABA. The dilution ratio of the secondary antibodies was 1:200 (NOS, NPY, SST) or 1:500 (GABA). The labeled sections were preserved in Vectashield mounting medium (Vector Laboratories) under coverslips.

Thionin staining. The tissue sections were mounted on Superfrost Plus slides (Fisher Thermo Scientific) and dried overnight in a 37°C oven. Following hydration of the tissue sections with gradually decreasing concentration of ethanol, sections were stained for thionin (Fisher). The tissue sections were then dehydrated with gradually increasing concentration of ethanol and cleared with xylene. Finally, cover slips were applied with Permount (Fisher).

Quantitative analysis. All analytical methods used here were as described previously in detail [24, 32, 75]. For the quantitative analysis of laminar distribution, NOS-IR neurons were photographed using a Zeiss Axioplan microscope with a 20× Zeiss Plan-Apochromat objective (Carl Zeiss Meditec). The laminar distribution was determined from the analysis of 144 neurons in nine sections, each with a width of 2000 μm, from three gerbils (three tissue sections from each animal). Morphological types were determined based on the analysis of 146 neurons in nine sections from three gerbils (three tissue sections from each animal). The analysis was carried out using 20× or 40× Zeiss Plan-Apochromat objectives. The mean diameter and area of NOS-IR neurons were determined based on the analysis of 114 neurons in twelve sections from three gerbils (four tissue sections from each animal). Cell profiles containing a nucleus and at least a faintly visible nucleolus were exclusively included in this analysis. The analysis was carried out using a 40× Zeiss Plan--Apochromat objective. The number of double-labeled neurons for NPY, SST, and GABA was counted in nine sections from three gerbils (three tissue sections from each animal). NOS--IR neurons were image on a computer monitor using a Zeiss Axioplan microscope with 40× and 63× Zeiss Plan-Apochromat objectives, and the cells were then drawn on acetate paper. The final images were drawn using Adobe Photoshop CS (Adobe Systems, San Jose, CA, USA).

Results

Laminar distribution of NOS-IR neurons

Fig. 1 depicts the cortical lamination and laminar distribution of NOS-IR neurons in the visual cortex of the gerbil. We visualized the cortical lamination using thionin staining (Figs. 1A, C) and the laminar distribution using DAB staining (Fig. 1B) or fluorescent staining (Fig. 1D). NOS-IR neurons were distributed throughout layers II–VI, with the densest concentration of NOS-IR neurons being observed in layer V. Fig. 2 provides a quantitative histogram of cell distribution revealing the density of NOS-IR neurons in each layer. The frequency of labeled neurons was different among the layers: 0% ± 0% of NOS-IR neurons were observed in layer I, 3.47% ± 3.60% in layer II, 11.11% ± 9.84% in layer III, 16.67% ± 9.33% in layer IV, 50.00% ± ± 11.11% in layer V, and 18.75% ± 13.16% in layer VI.

Morphology of NOS-IR neurons

NOS-IR neurons were intensely labeled in the visual cortex of the gerbil, with no weakly labeled neurons being detected. There were diverse morphological types in the gerbil visual cortex, including multipolar round/oval, multipolar stellate, vertical fusiform, horizontal, and pyriform cells (Fig. 3). The majority of NOS-IR neurons were round/oval cells, as reported in Figs. 3A–C, and 3K. Round/oval cells exhibited

Folia Histochem Cytobiol. 2024
DOI: 10.5603/fhc.99227
ISSN 0239-8508, e-ISSN 1897-5631

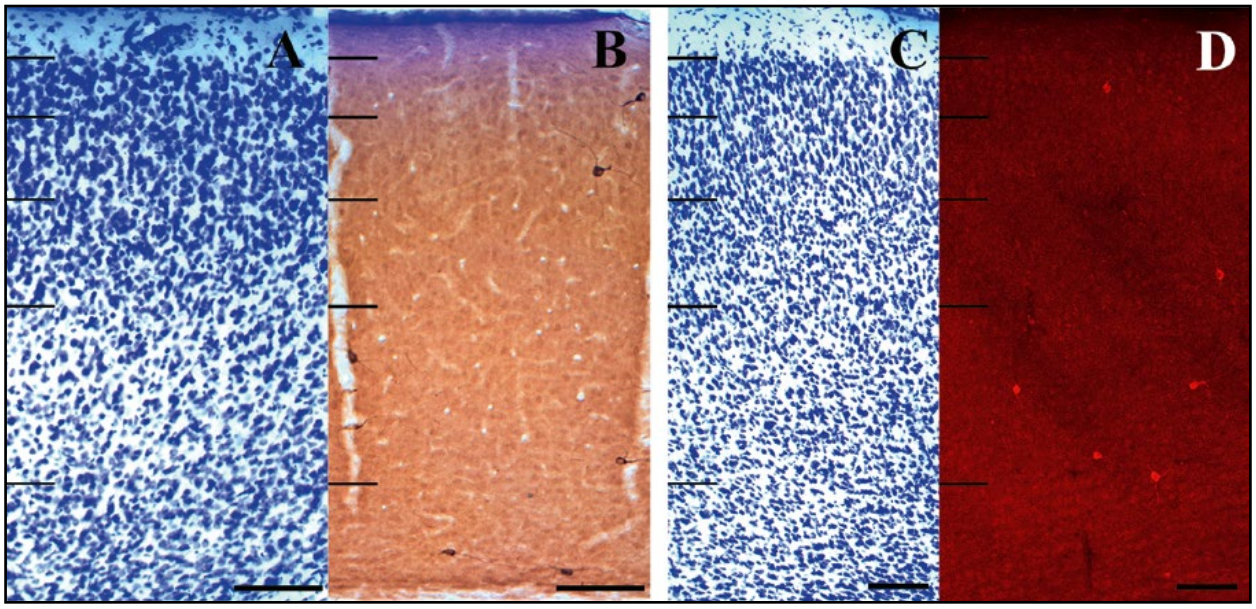

Figure 1. Low-magnification micrograph of the laminar distribution of NOS-IR neurons in the visual cortex of the gerbil. **A, C.** Thionin-stained sections showing cortical lamination. **B.** DAB-stained light micrograph of NOS-IR neurons. **D.** Fluorescence confocal micrograph of NOS-IR neurons. NOS-IR neurons were detected in only a small fraction of neurons within the gerbil visual cortex. Most NOS-IR neurons were in the deep cortical layers. Scale bar = 100 μm.

a round-/oval-shaped cell body and multiple dendrites extending in various directions. Stellate cells with a polygonal-shaped cell body and multiple dendrites extending in various directions are depicted in Fig. 3D, arrow in 3E, and 3L, respectively. In general, the cell bodies of round/oval cells were smaller than those of stellate cells. Figs. 3F, 3G, and 3M depict vertical fusiform cells with a vertical fusiform cell body, a primary long process ascending toward the pial surface, and a descending process. In turn, Figs. 3H, 3I, and 3N show horizontal cells with a horizontal fusiform cell body and horizontally oriented processes. Moreover, pyriform cells with a pear-shaped cell body and a thick, proximal dendritic stump directed superficially or horizontally toward the pial surface with a bouquet of dendrites are depicted in Figs. 3J and 3O. Finally, Fig. 4A provides a histogram of the relative frequency of each cell type. Quantitatively, 60.96% ± 10.28% [mean ± standard deviation (S.D.)] (89 of 146 cells) of NOS-IR neurons were round/oval, 14.38% ± 9.09% (21 of 146 cells) were stellate, 10.27% ± 7.45% (15 of 146 cells) were vertical fusiform, 8.90% ± 4.22% (13 of 146 cells) were horizontal, and 5.48% ± 3.40% (8 of 146 cells) were pyriform cells.

The average diameter and area of NOS-IR neurons in the visual cortex of the gerbil are reported in Figs. 4B, and 4C, respectively. The mean diameters of 114 NOS-IR neurons measured in 12 sections from three animals ranged from 10.3 to 17.44 μm, with a mean diameter of 13.79 μm (S.D. = 1.28 μm). The majority of the cells (79.82%, 91 out of 114 cells) were smaller than 15.00 μm. Furthermore, no NOS-IR neurons greater than 18 μm in diameter were detected in the gerbil visual cortex. Finally, these cells ranged in area from 83.26 to 238.79 μm², with a mean area of 150.57 μm² (S.D. = 28.20 μm²).

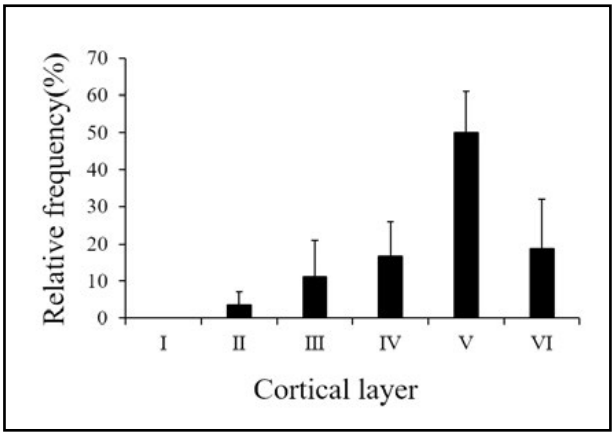

Figure 2. Histogram of the laminar distribution of NOS-IR neurons in the visual cortex of the gerbil. NOS-IR neurons were distributed through layers II–VI. There were no NOS-IR neurons in layer I, and most NOS-IR neurons were located in the deep cortical layers. The highest density of NOS-IR neurons was observed in layer V. The error bars represent standard deviations.

Colocalization of NOS with NPY, SST, and GABA

In this study, we examined whether NOS-IR neurons in the visual cortex of the gerbil were co-labeled with NPY, SST, and GABA. Fig. 5 depicts cells labeled

Folia Histochem Cytobiol. 2024
DOI: 10.5603/fhc.99227
ISSN 0239-8508, e-ISSN 1897-5631

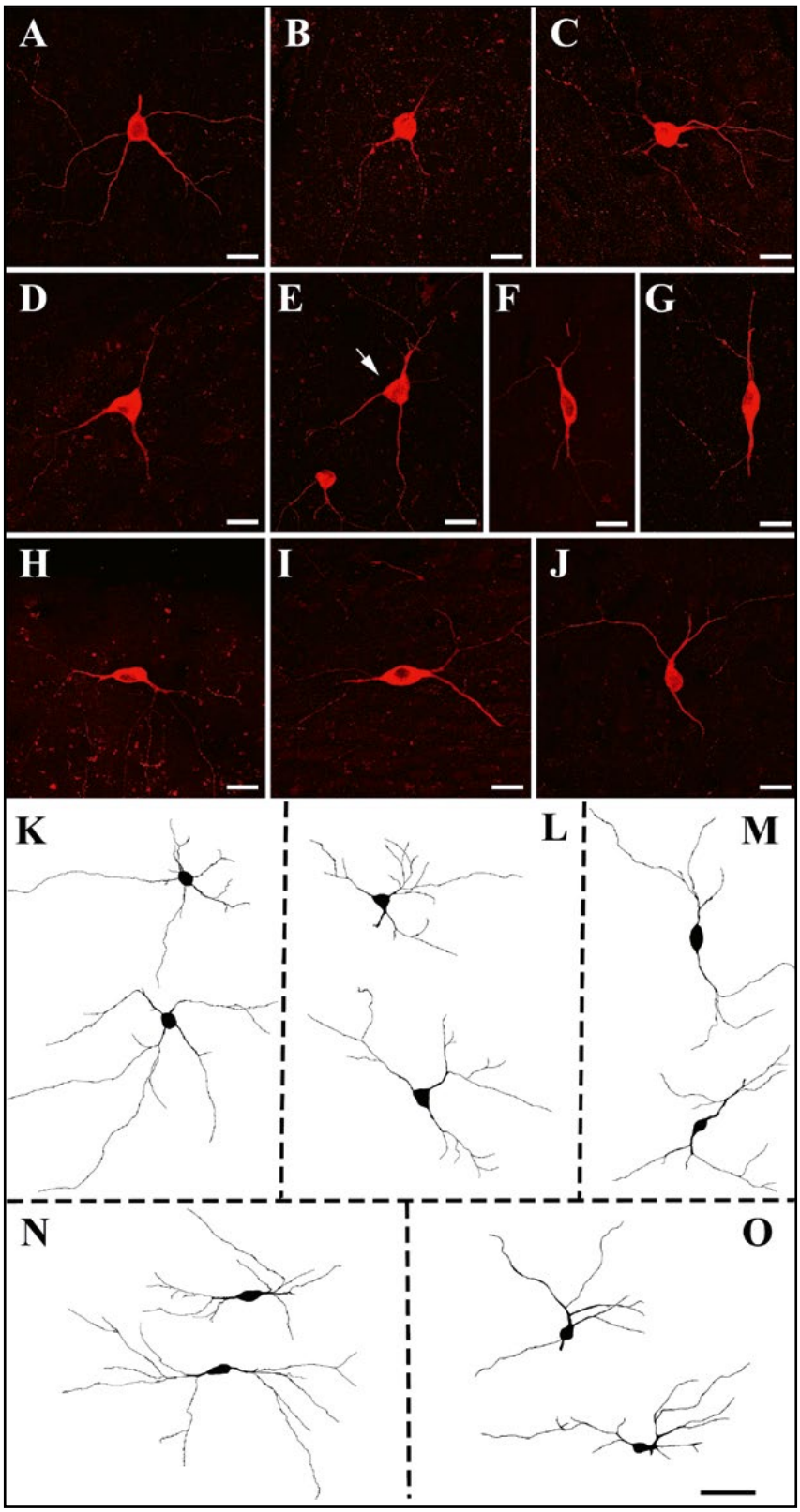

Figure 3. Morphology of NOS-IR neurons in the visual cortex of the gerbil, as represented in fluorescence confocal micrographs **(A–J)** and drawings **(K–O)** of NOS-IR neurons. **A–C**, and **K.** Multipolar round/oval cells. Most NOS-IR neurons are round/oval cells with many dendrites extending in all directions. **D**, arrow in **E** and **L**. Multipolar stellate cells. **F, G**, and **M.** Vertical fusiform cells with their longitudinal axis perpendicular to the pial surface. **H, I,** and **N.** Horizontal cells have a horizontal spindle-shaped cell body with horizontally oriented protrusions. **J**, and **O.** Pyriform cells with a thick primary dendrite oriented superficially or horizontally toward the pial surface. This ascending process had many small branches, forming a dendritic bouquet. Scale bars = = 20 μm (A–J), 50 μm (K–O).

Folia Histochem Cytobiol. 2024
DOI: 10.5603/fhc.99227
ISSN 0239-8508, e-ISSN 1897-5631

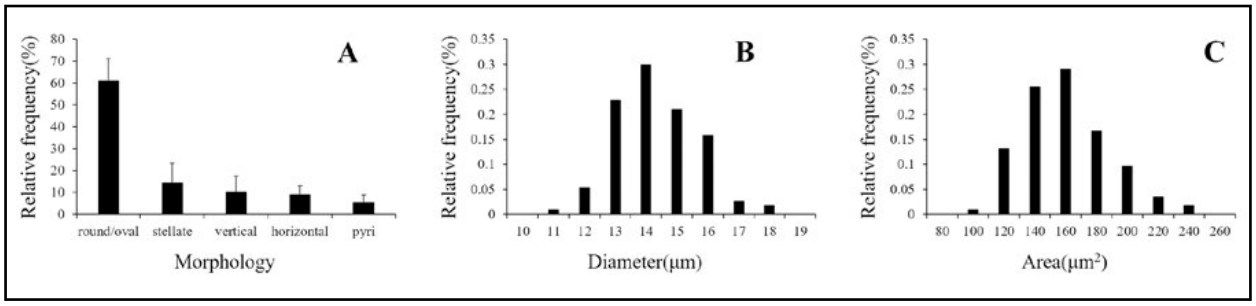

Figure 4. Histogram of the morphological distribution of NOS-IR neurons in the visual cortex of the gerbil. **A.** Most of the NOS-IR neurons were round/oval cells, whereas pyriform cells represented the smallest proportion of these neurons. The error bars represent standard deviations. Histogram of the diameter (**B**) and area (**C**) of 114 NOS-IR neurons in the gerbil visual cortex. The mean diameter of the neurons was 13.79 μm (SD = 1.28 μm), and their mean area was 150.57 μm² (SD = 28.20 μm²).

with NOS (Figs. 5 A1, B1, C1, D1, E1, F1), NPY (Figs. 5 A2, B2), SST (Figs. 5 C2, D2), and GABA (Figs. 5 E2, F2), as well as merged images of NOS staining with NPY (Figs. 5 A3, B3), SST (Figs. 5 C3, D3), and GABA (Figs. 5 E3, F3) staining. All NOS-IR neurons were double labeled with NPY (arrows in Figs. 5 A3, B3), but not all NPY-IR neurons were double labeled with NOS (arrowhead in Fig. 5 B3). Moreover, all NOS-IR neurons were double labeled with SST (arrows in Figs. 5 C3, D3), but not all SST-IR neurons were double labeled with NOS (arrowhead in Fig. 5 D3). Most of the NOS-IR neurons were not double labeled with GABA (arrowheads in Figs. 5 E3, F3), whereas many NOS-IR neurons were double labeled with GABA (arrow in Fig. 5 E3). Quantitatively, 100% ± ± 0% (139 of 139 cells) of NOS-IR neurons were double labeled with NPY, 100% ± 0% (147 of 147 cells) of NOS-IR neurons were double labeled with SST, and 34.55% ± 3.20% (38 of 110 cells) of NOS-IR neurons were double labeled with GABA. The percentage of double-labeled cells was relatively consistent across sections and among animals (Table 1).

Discussion

Our study showed that the highest number of NOS-IR neurons was observed in layer V. The labeled neurons exhibited various morphologies, with multipolar round/oval cells being predominant in the visual cortex of the gerbil. All NOS-IR neurons co-expressed NPY and SST, whereas only one-third of NOS-IR neurons co-expressed GABA.

Previous studies have demonstrated the existence of two types of NOS-IR neurons in the mammalian cerebral cortex according to staining intensity: intensely labeled type 1 cells and weakly labeled type 2 cells [12, 14, 37, 38, 76]. The present study, which examined the visual cortex of gerbils, showed that intensely labeled NOS-IR neurons were distributed through layers II–VI, with the highest density of the neurons in the infragranular layers, especially in layer V. No weakly labeled NOS-IR neurons were found in this study that was also reported for the visual cortex of the hamster [15]. Intensely labeled NOS-IR neurons are largely expressed in the infragranular layers in many mammals [12, 14, 15]. Thus, in monkeys [12], rabbits [14], hamsters [15], and mice [14], the highest density of intensely labeled NOS-IR neurons in the visual cortex is detected in layer VI. However, there are some discrepancies regarding the location of the highest density of intensely labeled NOS-IR neurons among animals; in the human visual cortex, intensely labeled NOS-IR neurons are mostly distributed in layers II/III [11], whereas in the rat visual cortex, intensely labeled NOS-IR neurons are usually located in layers II/III, V, and VI [18]. On the contrary, in the bat visual cortex, the highest density of intensely labeled NOS-IR neurons is found in layer IV [19]. Conversely, weakly labeled NOS-IR neurons are predominantly found in supragranular layers in many mammals [12, 14, 18]. In monkeys [12], rabbits [14], rats [18] and mice [14], the highest density of weakly labeled NOS-IR neurons is observed in layers II/III. However, there are also discrepancies according to species. For example, in the human visual cortex, weakly labeled NOS-IR neurons are mostly distributed in layer IV [11]. In the bat visual cortex, the highest density of weakly labeled NOS-IR neurons is found in layer VI [19]. Therefore, the present and previous studies indicate that there are labeling-intensity-specific and species--specific divergencies in the laminar distributions of NOS-IR neurons in the visual cortex of mammals. The anatomically different segregation of NOS-IR cells in the visual cortical layers suggests that there might be some subtle functional segregation of these cells as the input and output, and that the cortical cell types vary among the different cortical layers [77]. Although our understanding of the specific factors that contribute to this difference remains limited at present, our results provide an illustration of the diversity of

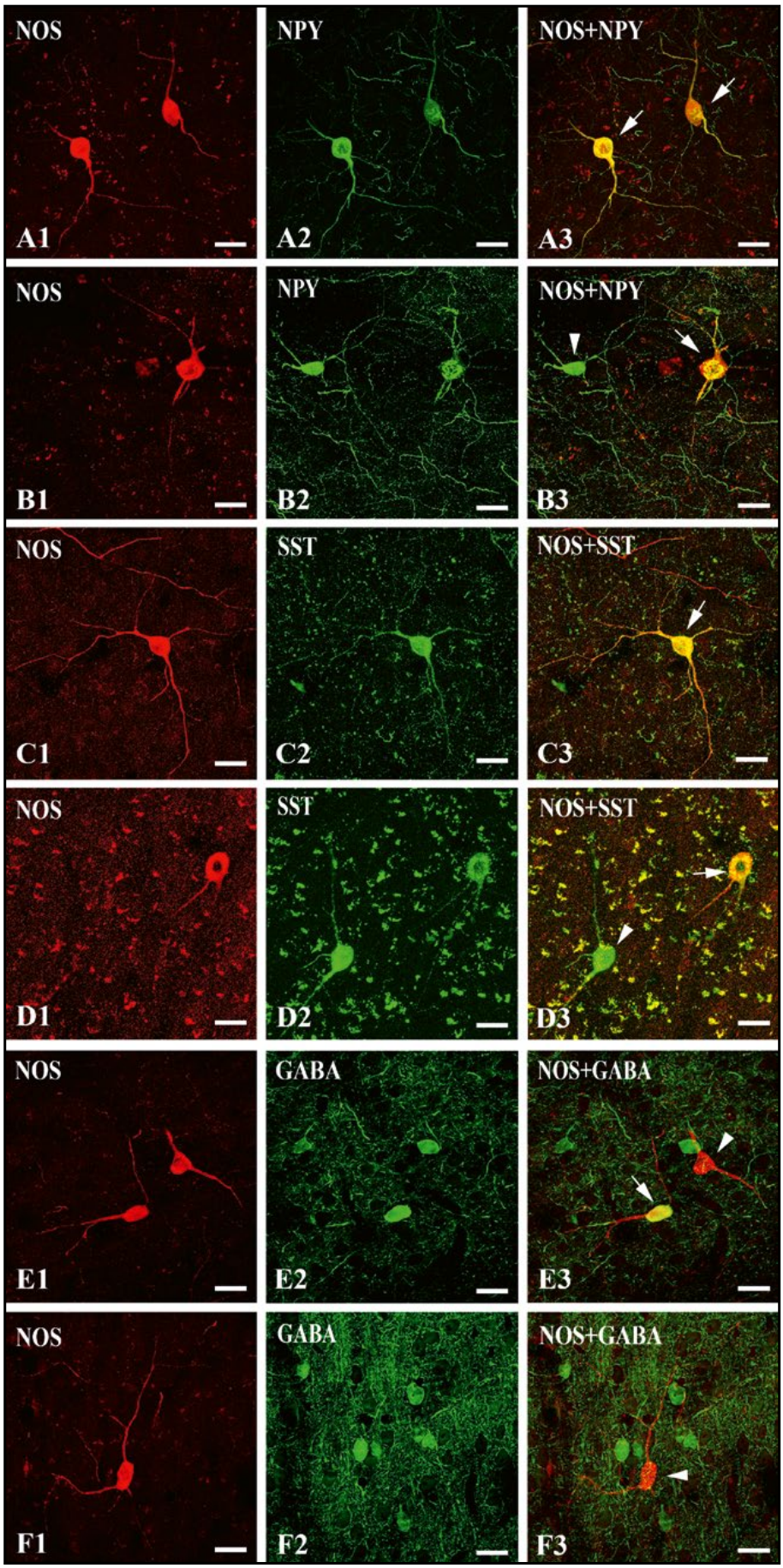

Figure 5. Colocalization of NOS--IR neurons with NPY, SST, and GABA in the visual cortex of the gerbil. Fluorescence confocal micrographs of NOS-IR neurons (A1, B1, C1, D1, E1, F1), shown in red, or NPY-IR (A2, B2), SST--IR (C2, D2), and GABA-IR (E2, F2) neurons, shown in green, and superimposed images of NOS with NPY (A3, B3), SST (C3, D3), and GABA (E3, F3) in the gerbil visual cortex. All NOS-IR neurons co-expressed NPY (arrows in A3, B3) or SST (arrow in C3, D3), but not all NPY (arrowhead in B3) or SST (arrowhead in D3) neurons. Many NOS-IR neurons co-expressed GABA (arrow in E3), but most did not (arrowhead in E3, F3). Scale bar = 20 μm.

Folia Histochem Cytobiol. 2024
DOI: 10.5603/fhc.99227
ISSN 0239-8508, e-ISSN 1897-5631

Table 1. Percentage of NOS-IR neurons and neurons double labeled with NPY, SST, or GABA in the gerbil visual cortex

Antibodies	Animal	No. of sections	No. of NOS cells	No. of Double	% Double (Mean ± SD)
NPY	#1	3	35	35	100 ± 0
	#2	3	45	45	100 ± 0
	#3	3	59	59	100 ± 0
NPY total		9	139	139	100 ± 0
SST	#1	3	51	51	100 ± 0
	#2	3	48	48	100 ± 0
	#3	3	48	48	100 ± 0
SST total		9	147	147	100 ± 0
GABA	#1	3	29	10	34.48 ± 4.04
	#2	3	38	13	34.21 ± 3.92
	#3	3	43	15	34.88 ± 2.96
GABA total		9	110	38	34.55 ± 3.20

2,000-μm width per section; Abbreviation: SD — standard deviation.

the distribution of NOS-IR neurons in the mammalian visual cortex.

The NOS-IR neurons in the visual cortex of the gerbil were a morphologically diverse subpopulation of nonpyramidal neurons; although most were multipolar round/oval cells, some multipolar stellate, vertical fusiform, horizontal, and pyriform cells were also observed. Here, NOS was not expressed in pyramidal neurons. Consistent with the current findings, in the visual cortex of humans [11], monkeys [12], rabbits [14], rats [17, 18], bats [19], hamsters [15, 78], and mice [14], most NOS-IR neurons were round/oval, and stellate cells with multipolar or bitufted dendritic arrangements and resembled nonpyramidal neurons. In other cortical areas, NADPH-diaphorase or NOS-IR neurons were also nonpyramidal neurons, indicating that NOS-IR neurons are a subpopulation of nonpyramidal cells in the mammalian cerebral cortex [79]. Our results validate the findings of previous studies and strongly suggest that NOS-IR neurons in the visual cortex of gerbils are not projecting neurons; rather, they function as interneurons like in humans [11], monkeys [12, 13], rabbits [14], bats [19], hamsters [15], mice [14].

Here, we also estimated the size of NOS-IR neurons and found that most NOS-IR neurons in the visual cortex of the gerbil exhibited a small to medium size (Figs. 4B and C), with a mean diameter of 13.79 ± ± 1.28 μm. In previous studies, the average diameter of intensely labeled NOS-IR neurons in most studied animals was less than 20 μm. In humans [11], rabbits [14], bats [19], and hamsters [15], the average diameter of intensely labeled NOS-IR neurons in the visual cortex was reported at 16 μm, 10–15 μm, 12 μm, and 10–15 μm, respectively. Thus, similar to that observed in other animals, the NOS-IR neurons in the visual cortex of the gerbil showed a typical small to medium size. In contrast, in the monkey cerebral cortex, including the visual cortex, the average diameter of intensely labeled NOS-IR neurons is 20–50 μm, and the average diameter of weakly labeled neurons is less than 20 μm [38]. Furthermore, in the human inferior colliculus, NOS-IR neurons were categorized into four types based on their perikaryal diameter, exhibiting a wide range of sizes, from 7 to 45 μm in diameter [80]. The data suggest that the size of NOS-IR cells may vary according to the species and brain areas and the small cells in the human inferior colliculus are morphologically similar to cells in the visual cortex of gerbil in the present study. Further studies to elucidate the relationship between this discrepancy in size and various functional aspects of NOS-IR neurons are indispensable in the future.

We compared the distributional pattern of NOS-IR neurons in the visual cortex of gerbils with that of other neurochemical markers, *i.e.*, NPY [24] and SST [32]. Notably, we found that the pattern of NOS-IR neurons was similar to that of NPY-IR and SST-IR neurons. Moreover, all of these neurons were distributed in layers II–VI and were primarily distributed in deep cortical layers, with the highest density detected in layer V. The majority of the NOS-IR, NPY-IR [24], and SST-IR neurons [32] were multipolar round/oval and multipolar stellate cells. Based on the analysis of the laminar distribution patterns and morphological types, NOS-IR, NPY-IR, and SST-IR neurons exhibit certain similarities.

To understand further the relationship between NOS-IR, NPY-IR, and SST-IR neurons in the visual cortex of the gerbil, we examined the double labeling of NOS with NPY and SST. The resulting data allowed us to draw the reliable conclusion that 100% of NOS--IR neurons co-expressed NPY and SST in the gerbil visual cortex. However, not all NPY-IR or SST-IR

neurons co-expressed NOS. In previous studies, NOS--IR neurons co-expressing NPY and SST were reported in the human prefrontal cortex [81], monkey cerebral cortex [37], rat striatum [82], and mouse barrel cortex [76]. Similar to our result, in monkey cerebral cortex [37], and rat striatum [82], not all NPY-IR and SST-IR neurons co-expressed NOS. In the cerebral cortex of monkeys, type 1 cells were essentially always (> 99%) immunoreactive to NPY and SST, whereas type 2 cells were rarely or never labeled with antibodies against NPY (< 2%) or SST (< 5%), demonstrating that the two types of nNOS-expressing cells can be distinguished using NPY and SST staining [37]. Similarly, in the mouse barrel cortex, most of the type 1 cells (91.5%) co-expressed SST, whereas a relatively low percentage of type 2 cells (18.7%) co-expressed SST [76]. Thus, considering the staining intensity and the co-expression pattern with NPY and SST observed in the present study, it is plausible to suggest that NOS--IR neurons present in the visual cortex of the gerbil are type 1 cells. In addition, the combined results of the laminar distribution, morphology, and double--labeling ratio of NOS-IR neurons with NPY-IR and SST-IR neurons suggest that the NOS-IR neurons are a subpopulation of NPY-IR and/or SST-IR neurons in the visual cortex of gerbils.

Notably, based on the double-labeling data of NOS and GABA, only approximately one third of NOS-IR neurons expressed GABA in the visual cortex of the gerbil. This result was interesting to us because previous studies reported that NOS-IR neurons are mostly subpopulations of GABAergic neurons [16, 38, 39], and the NOS-IR neurons in the present study were nonpyramidal interneurons that co-expressed NPY and SST, which are commonly used as chemical markers for GABAergic subpopulations in rats [39] and mice [83, 84]. However, a previous study of the rat hippocampus reported a different pattern of GABA expression in NOS-IR neurons across subregions of the hippocampus [39]. In the rat dentate gyrus and Ammon's horn outside the pyramidal layer, all NOS-IR neurons co-expressed GABA; however, in the pyramidal layer of Ammon's horn and alveus, no NOS-IR neurons co-expressed GABA [39]. In the monkey visual cortex, although all type 2 NOS-IR neurons co-expressed GABA, many type 1 NOS-IR neurons (42%) did not co-express GABA [38], indicating the differential regional- and type-specific co-expression of NOS-IR neurons with GABA. In addition, although SST-IR neurons are thought to be almost GABAergic in the visual cortex [85], we previously found that only one-third of SST-IR neurons expressed GABA in the gerbil visual cortex [32]. Therefore, we suggested the existence of an unconventional group of SST neurons that do not express GABA [32]. In addition, NPY-IR neurons are thought to be GABAergic mainly in the cerebral cortex [86–89], hippocampus [90], and hypothalamus [91]. However, in a previous study [24], at least 10% of the NPY-IR neurons in the gerbil visual cortex did not express GABA. It is notable that, although calcium-binding proteins are conventionally used as chemical markers of GABAergic subpopulations, which account for the majority of the total GABAergic population in rats and mice [16, 85], they expressed a low ratio of double labeling with GABA in the gerbil visual cortex [75]. This suggests that the expression patterns of various chemical markers in the visual cortex are species-specific even in the rodents, possibly providing a basis for understanding subtle functional differences in the future. However, additional physiological studies are needed to clarify this issue.

NO is involved in various multifunctional processes and pathologies because of the widespread expression of NOS in the CNS and the fact that NO has extensive and unique opportunities to interact with other neuronal components [5]. In the mammalian visual cortex, previous studies have revealed potential roles for NO in various processes, such as the synaptic transmission [92], homeostatic plasticity [93], apoptosis [94] and neurovascular coupling [95]. In the mouse visual cortex, NO-stimulated cGMP formation is essential for the activity-dependent strengthening of synaptic transmission [92]. In the rat visual cortex, homeostatic plasticity processes, which involve the integration of new information in a neuron by changing the strength of its synaptic input while maintaining its stable excitability level, require nNOS activation [93]. In the visual cortex of the golden hamster, NOS inhibition significantly rescued neurons from undergoing apoptosis, indicating that NO may serve as a signal that triggers apoptosis and plays a role in the maturation of the visual cortex [94]. In addition, in the dynamic control of cerebral blood flow in humans, the speed of the neurovascular coupling responses to visual stimulation is reduced by nNOS inhibition [95]. However, to date, there have been relatively few studies of the subregional- and cell type-specific functions of nNOS in the visual cortex. Further research is needed to delineate the specific function of nNOS and its correlation with different cell types. The present data may serve as a foundation for elucidating the diverse roles of NOS-IR neurons in the mammalian visual cortex.

In conclusion, the current findings suggest that, although laminar organization is distinctive across species, the morphological characteristics of NOS-IR neurons in the visual cortex of gerbils are similar to those of other species. Double labeling of NOS-IR neurons with NPY and SST showed that NOS-IR neurons

Folia Histochem Cytobiol. 2024
DOI: 10.5603/fhc.99227
ISSN 0239-8508, e-ISSN 1897-5631

are a subpopulation of NPY-IR and/or SST-IR neurons. However, NOS-IR neurons exhibited a low percentage of double labeling with GABA in the visual cortex of the gerbil. Although the specific function of NO in the gerbil visual cortex cannot be confirmed at present, the specific laminar organization, morphological features of NOS-IR neurons, and different colocalization patterns of NOS-IR neurons with other chemical markers across species likely reflect the functional diversity of NO in visual activities. These data will provide valuable clues for a better understanding of NO function and species diversity.

Article information and declarations

Data availability statement

The datasets used and/or analyzed during the current study are available from the corresponding author on reasonable request.

Ethics statement

All animal experiments were approved by the committee of Kyungpook National University (permission NO. 2023-0317). Guide for the Care and Use of Laboratory Animals (https://grants.nih.gov/grants/olaw/guide-for-the-care-and-use-of-laboratory-animals.pdf) were followed.

Author contributions

XYK, GJJ and CJJ designed the research study. XYK and GJJ performed the research. XYK and GJJ analyzed the data. XYK, GJJ and CJJ wrote the manuscript. All authors contributed to editorial changes in the manuscript. All authors read and approved the final manuscript.

Funding

This research was supported by Basic Science Research Program through the National Research Foundation of Korea (NRF) funded by Ministry of Education (NRF-2020R1F1A1069293 and NRF-2016R1A-6A1A05011910).

Conflict of interest

The authors declare that there are no conflict of interest.

References

1. Getting SJ, Segieth J, Ahmad S, et al. Biphasic modulation of GABA release by nitric oxide in the hippocampus of freely moving rats in vivo. Brain Res. 1996; 717(1-2): 196–199, doi: 10.1016/0006-8993(96)00127-8, indexed in Pubmed: 8738273.
2. Kopp-Scheinpflug C, Forsythe ID. Nitric oxide signaling in the auditory pathway. Front Neural Circuits. 2021; 15: 759342, doi: 10.3389/fncir.2021.759342, indexed in Pubmed: 34712124.
3. Poon CH, Tsui KC, Chau SC, et al. Functional roles of neuronal nitric oxide synthase in neurodegenerative diseases and mood disorders. Curr Alzheimer Res. 2021; 18(10): 831–840, doi: 10.2174/1567205018666211022164025, indexed in Pubmed: 34719364.
4. Tricoire L, Vitalis T. Neuronal nitric oxide synthase expressing neurons: a journey from birth to neuronal circuits. Front Neural Circuits. 2012; 6: 82, doi: 10.3389/fncir.2012.00082, indexed in Pubmed: 23227003.
5. Zhou Li, Zhu DY. Neuronal nitric oxide synthase: structure, subcellular localization, regulation, and clinical implications. Nitric Oxide. 2009; 20(4): 223–230, doi: 10.1016/j.niox.2009.03.001, indexed in Pubmed: 19298861.
6. Ghimire K, Altmann HM, Straub AC, et al. Nitric oxide: what's new to NO? Am J Physiol Cell Physiol. 2017; 312(3): C254–C262, doi: 10.1152/ajpcell.00315.2016, indexed in Pubmed: 27974299.
7. Picón-Pagès P, Garcia-Buendia J, Muñoz FJ. Functions and dysfunctions of nitric oxide in brain. Biochim Biophys Acta Mol Basis Dis. 2019; 1865(8): 1949–1967, doi: 10.1016/j.bbadis.2018.11.007, indexed in Pubmed: 30500433.
8. Zhang Y, Li N, Yang Z. Perinatal food restriction impaired spatial learning and memory behavior and decreased the density of nitric oxide synthase neurons in the hippocampus of adult male rat offspring. Toxicol Lett. 2010; 193(2): 167–172, doi: 10.1016/j.toxlet.2010.01.002, indexed in Pubmed: 20079408.
9. Koylu EO, Kanit L, Taskiran D, et al. Effects of nitric oxide synthase inhibition on spatial discrimination learning and central DA2 and mACh receptors. Pharmacol Biochem Behav. 2005; 81(1): 32–40, doi: 10.1016/j.pbb.2005.02.008, indexed in Pubmed: 15894061.
10. Džoljić E, Grbatinić I, Kostić V. Why is nitric oxide important for our brain? Funct Neurol. 2015; 30(3): 159–163, doi: 10.11138/fneur/2015.30.3.159, indexed in Pubmed: 26910176.
11. Lüth HJ, Hedlich A, Hilbig H, et al. Morphological analyses of NADPH-diaphorase/nitric oxide synthase positive structures in human visual cortex. J Neurocytol. 1994; 23(12): 770–782, doi: 10.1007/BF01268089, indexed in Pubmed: 7534823.
12. Aoki C, Fenstemaker S, Lubin M, et al. Nitric oxide synthase in the visual cortex of monocular monkeys as revealed by light and electron microscopic immunocytochemistry. Brain Res. 1993; 620(1): 97–113, doi: 10.1016/0006-8993(93)90275-r, indexed in Pubmed: 7691382.
13. Wiencken AE, Casagrande VA. The distribution of NADPH diaphorase and nitric oxide synthetase (NOS) in relation to the functional compartments of areas V1 and V2 of primate visual cortex. Cereb Cortex. 2000; 10(5): 499–511, doi: 10.1093/cercor/10.5.499, indexed in Pubmed: 10847600.
14. Lee JE, Jeon CJ. Immunocytochemical localization of nitric oxide synthase-containing neurons in mouse and rabbit visual cortex and co-localization with calcium-binding proteins. Mol Cells. 2005; 19(3): 408–417, indexed in Pubmed: 15995359.
15. Lee JE, Ahn CH, Lee JY, et al. Nitric oxide synthase and calcium-binding protein-containing neurons in the hamster visual cortex. Mol Cells. 2004; 18(1): 30–39, indexed in Pubmed: 15359121.
16. Gonchar Y, Burkhalter A. Three distinct families of GABAergic neurons in rat visual cortex. Cereb Cortex. 1997; 7(4): 347–358, doi: 10.1093/cercor/7.4.347, indexed in Pubmed: 9177765.
17. Cha CI, Uhm MR, Shin DH, et al. Immunocytochemical study on the distribution of NOS-immunoreactive neurons in the cerebral cortex of aged rats. Neuroreport. 1998; 9(10): 2171–2174, doi: 10.1097/00001756-199807130-00004, indexed in Pubmed: 9694194.
18. Yousef T, Neubacher U, Eysel UT, et al. Nitric oxide synthase in rat visual cortex: an immunohistochemical study. Brain Res

Brain Res Protoc. 2004; 13(1): 57–67, doi: 10.1016/j.brainresprot.2004.01.004, indexed in Pubmed: 15063842.
19. Gu YN, Kim HG, Jeon CJ. Localization of nitric oxide synthase-containing neurons in the bat visual cortex and co-localization with calcium-binding proteins. Acta Histochem Cytochem. 2015; 48(4): 125–133, doi: 10.1267/ahc.14066, indexed in Pubmed: 26379314.
20. Tatemoto K. Neuropeptide Y: complete amino acid sequence of the brain peptide. Proc Natl Acad Sci U S A. 1982; 79(18): 5485–5489, doi: 10.1073/pnas.79.18.5485, indexed in Pubmed: 6957876.
21. Greene ES, Abdelli N, Dridi JS, et al. Avian neuropeptide Y: beyond feed intake regulation. Vet Sci. 2022; 9(4), doi: 10.3390/vetsci9040171, indexed in Pubmed: 35448669.
22. Tanaka M, Yamada S, Watanabe Y. The role of neuropeptide Y in the nucleus accumbens. Int J Mol Sci. 2021; 22(14), doi: 10.3390/ijms22147287, indexed in Pubmed: 34298907.
23. Alviña K, Jodeiri Farshbaf M, Mondal AK. Long term effects of stress on hippocampal function: emphasis on early life stress paradigms and potential involvement of neuropeptide Y. J Neurosci Res. 2021; 99(1): 57–66, doi: 10.1002/jnr.24614, indexed in Pubmed: 32162350.
24. Lee MJ, Lee WT, Jeon CJ. Organization of neuropeptide Y-immunoreactive cells in the Mongolian gerbil (Meriones unguiculatus) visual cortex. Cells. 2021; 10(2), doi: 10.3390/cells10020311, indexed in Pubmed: 33546356.
25. Strowski MZ, Blake AD. Function and expression of somatostatin receptors of the endocrine pancreas. Mol Cell Endocrinol. 2008; 286(1-2): 169–179, doi: 10.1016/j.mce.2008.02.007, indexed in Pubmed: 18375050.
26. Natan RG, Rao W, Geffen MN. Cortical interneurons differentially shape frequency tuning following adaptation. Cell Rep. 2017; 21(4): 878–890, doi: 10.1016/j.celrep.2017.10.012, indexed in Pubmed: 29069595.
27. Phillips EAK, Schreiner CE, Hasenstaub AR. Cortical interneurons differentially regulate the effects of acoustic context. Cell Rep. 2017; 20(4): 771–778, doi: 10.1016/j.celrep.2017.07.001, indexed in Pubmed: 28746863.
28. Riedemann T. Diversity and function of somatostatin-expressing interneurons in the cerebral cortex. Int J Mol Sci. 2019; 20(12), doi: 10.3390/ijms20122952, indexed in Pubmed: 31212931.
29. Song YH, Hwang YS, Kim K, et al. Somatostatin enhances visual processing and perception by suppressing excitatory inputs to parvalbumin-positive interneurons in V1. Sci Adv. 2020; 6(17): eaaz0517, doi: 10.1126/sciadv.aaz0517, indexed in Pubmed: 32494634.
30. Chen SX, Kim AN, Peters AJ, et al. Subtype-specific plasticity of inhibitory circuits in motor cortex during motor learning. Nat Neurosci. 2015; 18(8): 1109–1115, doi: 10.1038/nn.4049, indexed in Pubmed: 26098758.
31. Kossut M, Łukomska A, Dobrzański G, et al. Somatostatin receptors in the brain. Postepy Biochem. 2018; 64(3): 213–221, doi: 10.18388/pb.2018_133, indexed in Pubmed: 30656906.
32. Kwon KM, Lee MJ, Chung HS, et al. The organization of somatostatin-immunoreactive cells in the visual cortex of the gerbil. Biomedicines. 2022; 10(1), doi: 10.3390/biomedicines10010092, indexed in Pubmed: 35052772.
33. Crowley T, Cryan JF, Downer EJ, et al. Inhibiting neuroinflammation: the role and therapeutic potential of GABA in neuro-immune interactions. Brain Behav Immun. 2016; 54: 260–277, doi: 10.1016/j.bbi.2016.02.001, indexed in Pubmed: 26851553.
34. Koh W, Kwak H, Cheong E, et al. GABA tone regulation and its cognitive functions in the brain. Nat Rev Neurosci. 2023; 24(9): 523–539, doi: 10.1038/s41583-023-00724-7, indexed in Pubmed: 37495761.
35. Wu C, Sun D. GABA receptors in brain development, function, and injury. Metab Brain Dis. 2015; 30(2): 367–379, doi: 10.1007/s11011-014-9560-1, indexed in Pubmed: 24820774.
36. Pinto JGA, Hornby KR, Jones DG, et al. Developmental changes in GABAergic mechanisms in human visual cortex across the lifespan. Front Cell Neurosci. 2010; 4: 16, doi: 10.3389/fncel.2010.00016, indexed in Pubmed: 20592950.
37. Smiley JF, McGinnis JP, Javitt DC. Nitric oxide synthase interneurons in the monkey cerebral cortex are subsets of the somatostatin, neuropeptide Y, and calbindin cells. Brain Res. 2000; 863(1-2): 205–212, doi: 10.1016/s0006-8993(00)02136-3, indexed in Pubmed: 10773208.
38. Yan XX, Jen LS, Garey LJ. NADPH-diaphorase-positive neurons in primate cerebral cortex colocalize with GABA and calcium-binding proteins. Cereb Cortex. 1996; 6(3): 524–529, doi: 10.1093/cercor/6.3.524, indexed in Pubmed: 8670678.
39. Valtschanoff JG, Weinberg RJ, Kharazia VN, et al. Neurons in rat cerebral cortex that synthesize nitric oxide: NADPH diaphorase histochemistry, NOS immunocytochemistry, and colocalization with GABA. Neurosci Lett. 1993; 157(2): 157–161, doi: 10.1016/0304-3940(93)90726-2, indexed in Pubmed: 7694193.
40. Batchelder M, Keller LS, Sauer MB, et al. Gerbils. In: Suckow MA, Stevens KA, Wilson RP. ed. The laboratory rabbit, guinea pig, hamster, and other rodents. Elsevier, Amsterdam 2012: 1131–1155.
41. Cheal ML. The gerbil: a unique model for research on aging. Exp Aging Res. 1986; 12(1): 3–21, doi: 10.1080/03610738608259430, indexed in Pubmed: 3519235.
42. Heeringa AN, Jüchter C, Beutelmann R, et al. Altered neural encoding of vowels in noise does not affect behavioral vowel discrimination in gerbils with age-related hearing loss. Front Neurosci. 2023; 17: 1238941, doi: 10.3389/fnins.2023.1238941, indexed in Pubmed: 38033551.
43. Zucão MI, Grigio V, Guerra LH, et al. Aging effects in adrenal cortex of male Mongolian gerbil: a model for endocrine studies. Steroids. 2024; 203: 109366, doi: 10.1016/j.steroids.2024.109366, indexed in Pubmed: 38242273.
44. Gordon S, Stolzenberg SJ, Cekleniak WP. Effects of cholesterol and beta-sitosterol in the gerbil. Am J Physiol. 1959; 197: 671–673, doi: 10.1152/ajplegacy.1959.197.3.671, indexed in Pubmed: 13851233.
45. Li YG, Yan ZC, Wang DH. Physiological and biochemical basis of basal metabolic rates in Brandt's voles (Lasiopodomys brandtii) and Mongolian gerbils (Meriones unguiculatus). Comp Biochem Physiol A Mol Integr Physiol. 2010; 157(3): 204–211, doi: 10.1016/j.cbpa.2010.06.183, indexed in Pubmed: 20601053.
46. Khakisahneh S, Zhang XY, Nouri Z, et al. Thyroid hormones mediate metabolic rate and oxidative, anti-oxidative balance at different temperatures in Mongolian gerbils (Meriones unguiculatus). Comp Biochem Physiol C Toxicol Pharmacol. 2019; 216: 101–109, doi: 10.1016/j.cbpc.2018.11.016, indexed in Pubmed: 30476595.
47. Mishra KK, Srivastava S, Aayyagari A, et al. Development of an animal model of Helicobacter pylori (Indian strain) infection. Indian J Gastroenterol. 2019; 38(2): 167–172, doi: 10.1007/s12664-018-0905-2, indexed in Pubmed: 30911993.
48. Ansari S, Yamaoka Y. Animal models and Helicobacter pylori infection. J Clin Med. 2022; 11(11): 3141, doi: 10.3390/jcm11113141, indexed in Pubmed: 35683528.
49. Kim H, Park JH, Shin MC, et al. Fate of astrocytes in the gerbil hippocampus after transient global cerebral ischemia. Int J Mol Sci. 2019; 20(4), doi: 10.3390/ijms20040845, indexed in Pubmed: 30781368.

50. Nilsson P, Ravinet M, Cui Y, et al. Polygenic plague resistance in the great gerbil uncovered by population sequencing. PNAS Nexus. 2022; 1(5): pgac211, doi: 10.1093/pnasnexus/pgac211, indexed in Pubmed: 36712379.
51. Quintar AA, Gonçalves BF, Taboga SR, et al. The mongolian gerbil (Meriones unguiculatus) as a model for inflammation-promoted prostate carcinogenesis. Cell Biol Int. 2017; 41(11): 1234––1238, doi: 10.1002/cbin.10789, indexed in Pubmed: 28493535.
52. Wroblewski LE, Peek RM. Clinical pathogenesis, molecular mechanisms of gastric cancer development. Curr Top Microbiol Immunol. 2023; 444: 25–52, doi: 10.1007/978-3-031-47331-9_2, indexed in Pubmed: 38231214.
53. Thomas H, Tillein J, Heil P, et al. Functional organization of auditory cortex in the mongolian gerbil (Meriones unguiculatus). I. Electrophysiological mapping of frequency representation and distinction of fields. Eur J Neurosci. 1993; 5(7): 882–897, doi: 10.1111/j.1460-9568.1993.tb00940.x, indexed in Pubmed: 8281300.
54. Depner M, Tziridis K, Hess A, et al. Sensory cortex lesion triggers compensatory neuronal plasticity. BMC Neurosci. 2014; 15: 57, doi: 10.1186/1471-2202-15-57, indexed in Pubmed: 24886276.
55. Henschke JU, Oelschlegel AM, Angenstein F, et al. Early sensory experience influences the development of multisensory thalamocortical and intracortical connections of primary sensory cortices. Brain Struct Funct. 2018; 223(3): 1165–1190, doi: 10.1007/s00429-017-1549-1, indexed in Pubmed: 29094306.
56. Keplinger S, Beiderbeck B, Michalakis S, et al. Optogenetic control of neural circuits in the Mongolian gerbil. Front Cell Neurosci. 2018; 12: 111, doi: 10.3389/fncel.2018.00111, indexed in Pubmed: 29740286.
57. Lee TK, Chen BH, Lee JC, et al. Agedependent decreases in insulinlike growth factorI and its receptor expressions in the gerbil olfactory bulb. Mol Med Rep. 2018; 17(6): 8161–8166, doi: 10.3892/mmr.2018.8886, indexed in Pubmed: 29658594.
58. Brugge JF, Poon PW, So AT, et al. Thermal images of somatic sensory cortex obtained through the skull of rat and gerbil. Exp Brain Res. 1995; 106(1): 7–18, doi: 10.1007/BF00241352, indexed in Pubmed: 8542979.
59. Bertorelli R, Adami M, Ongini E. The Mongolian gerbil in experimental epilepsy. Ital J Neurol Sci. 1995; 16(1-2): 101–106, doi: 10.1007/BF02229081, indexed in Pubmed: 7642342.
60. Kitabatake TT, Marini LC, Gonçalves RB, et al. Behavioral effects and neural changes induced by continuous and not continuous treadmill training, post bilateral cerebral ischemia in gerbils. Behav Brain Res. 2015; 291: 20–25, doi: 10.1016/j.bbr.2015.04.057, indexed in Pubmed: 25975174.
61. Lewczuk A, Boratyńska-Jasińska A, Zabłocka B. Validation of the reference genes for expression analysis in the hippocampus after transient ischemia/reperfusion injury in gerbil brain. Int J Mol Sci. 2023; 24(3), doi: 10.3390/ijms24032756, indexed in Pubmed: 36769080.
62. Thiessen DD, Goar S. Stereotaxic atlas of the hypothalamus of the Mongolian gerbil (Meriones unguiculatus). J Comp Neurol. 1970; 140(1): 123–127, doi: 10.1002/cne.901400108, indexed in Pubmed: 5459209.
63. Radtke-Schuller S, Schuller G, Angenstein F, et al. Brain atlas of the Mongolian gerbil (Meriones unguiculatus) in CT/MRI-aided stereotaxic coordinates. Brain Struct Funct. 2016; 221 Suppl 1(Suppl 1): 1–272, doi: 10.1007/s00429-016-1259-0, indexed in Pubmed: 27507296.
64. Mankin EA, Thurley K, Chenani A, et al. The hippocampal code for space in Mongolian gerbils. Hippocampus. 2019; 29(9): 787––801, doi: 10.1002/hipo.23075, indexed in Pubmed: 30746805.
65. Koolhaas JM. The laboratory rat. In: Hubrecht R, Kirkwood J. ed. The UFAW handbook on the care and management of laboratory and other research animals. 8th ed. John Wiley & Sons, Hoboken 2010: 311–326.
66. Suckow MA, Hashway S, Pritchett-Corning KR. The laboratory mouse. CRC press, Boca Raton 2023.
67. Bytyqi AH, Layer PG. Lamina formation in the Mongolian gerbil retina (Meriones unguiculatus). Anat Embryol (Berl). 2005; 209(3): 217–225, doi: 10.1007/s00429-004-0443-9, indexed in Pubmed: 15668778.
68. Govardovskii VI, Röhlich P, Szél A, et al. Cones in the retina of the Mongolian gerbil, Meriones unguiculatus: an immunocytochemical and electrophysiological study. Vision Res. 1992; 32(1): 19–27, doi: 10.1016/0042-6989(92)90108-u, indexed in Pubmed: 1502806.
69. Remé CE, Wirz-Justice A, Terman M. The visual input stage of the mammalian circadian pacemaking system: I. Is there a clock in the mammalian eye? J Biol Rhythms. 1991; 6(1): 5–29, doi: 10.1177/074873049100600104, indexed in Pubmed: 1773080.
70. Baker AG, Emerson VF. Grating acuity of the Mongolian gerbil (Meriones unguiculatus). Behav Brain Res. 1983; 8(2): 195–209, doi: 10.1016/0166-4328(83)90054-2, indexed in Pubmed: 6860462.
71. Huber G, Heynen S, Imsand C, et al. Novel rodent models for macular research. PLoS One. 2010; 5(10): e13403, doi: 10.1371/journal.pone.0013403, indexed in Pubmed: 20976212.
72. Jeong MJ, Jeon CJ. Localization of melanopsin-immunoreactive cells in the Mongolian gerbil retina. Neurosci Res. 2015; 100: 6–16, doi: 10.1016/j.neures.2015.06.002, indexed in Pubmed: 26083722.
73. Yang S, Luo X, Xiong G, et al. The electroretinogram of Mongolian gerbil (Meriones unguiculatus): comparison to mouse. Neurosci Lett. 2015; 589: 7–12, doi: 10.1016/j.neulet.2015.01.018, indexed in Pubmed: 25578951.
74. Macharadze T, Budinger E, Brosch M, et al. Early sensory loss alters the dendritic branching and spine density of supragranular pyramidal neurons in rodent primary sensory cortices. Front Neural Circuits. 2019; 13: 61, doi: 10.3389/fncir.2019.00061, indexed in Pubmed: 31611778.
75. Son JR, Kuai XY, Jeon CJ. Immunocytochemical localization of calbindin-D28K, calretinin, and parvalbumin in the Mongolian gerbil (Meriones unguiculatus) visual cortex. Folia Histochem Cytobiol. 2023; 61(2): 81–97, doi: 10.5603/FHC.a2023.0010, indexed in Pubmed: 37435896.
76. Perrenoud Q, Geoffroy H, Gauthier B, et al. Characterization of type I and type II nNOS-expressing interneurons in the barrel cortex of mouse. Front Neural Circuits. 2012; 6: 36, doi: 10.3389/fncir.2012.00036, indexed in Pubmed: 22754499.
77. Hirsch JA, Martinez LM. Laminar processing in the visual cortical column. Curr Opin Neurobiol. 2006; 16(4): 377–384, doi: 10.1016/j.conb.2006.06.014, indexed in Pubmed: 16842989.
78. Xiao YM, Diao YC, So KF. A morphological study of neurons expressing NADPH diaphorase activity in the visual cortex of the golden hamster. Brain Behav Evol. 1996; 48(4): 221–230, doi: 10.1159/000113200, indexed in Pubmed: 8886393.
79. Yan XX, Garey LJ. Morphological diversity of nitric oxide synthesising neurons in mammalian cerebral cortex. J Hirnforsch. 1997; 38(2): 165–172, indexed in Pubmed: 9176729.
80. Hinova-Palova D, Landzhov B, Dzhambazova E, et al. NADPH-diaphorase-positive neurons in the human inferior colliculus: morphology, distribution and clinical implications. Brain Struct Funct. 2017; 222(4): 1829–1846, doi: 10.1007/s00429-016-1310-1, indexed in Pubmed: 27646398.
81. Banovac I, Sedmak D, Esclapez M, et al. The Distinct Characteristics of Somatostatin Neurons in the Human Brain. Mol Neurobiol. 2022; 59(8): 4953–4965, doi: 10.1007/s12035-022-02892-6, indexed in Pubmed: 35665897.

82. Figueredo-Cardenas G, Morello M, Sancesario G, et al. Colocalization of somatostatin, neuropeptide Y, neuronal nitric oxide synthase and NADPH-diaphorase in striatal interneurons in rats. Brain Res. 1996; 735(2): 317–324, doi: 10.1016/0006-8993(96)00801-3, indexed in Pubmed: 8911672.
83. Jinno S, Kinukawa N, Kosaka T. Morphometric multivariate analysis of GABAergic neurons containing calretinin and neuronal nitric oxide synthase in the mouse hippocampus. Brain Res. 2001; 900(2): 195–204, doi: 10.1016/s0006-8993(01)02292-2, indexed in Pubmed: 11334798.
84. Jinno S, Aika Y, Fukuda T, et al. Quantitative analysis of neuronal nitric oxide synthase-immunoreactive neurons in the mouse hippocampus with optical disector. J Comp Neurol. 1999; 410(3): 398–412, indexed in Pubmed: 10404408.
85. Gonchar Y, Wang Q, Burkhalter A. Multiple distinct subtypes of GABAergic neurons in mouse visual cortex identified by triple immunostaining. Front Neuroanat. 2007; 1: 3, doi: 10.3389/neuro.05.003.2007, indexed in Pubmed: 18958197.
86. Dávila JC, de la Calle A, Gutiérrez A, et al. Distribution of neuropeptide Y (NPY) in the cerebral cortex of the lizards Psammodromus algirus and podarcis hispanica: co-localization of NPY, somatostatin, and GABA. J Comp Neurol. 1991; 308(3): 397–408, doi: 10.1002/cne.903080307, indexed in Pubmed: 1677949.
87. Hendry SH, Jones EG, DeFelipe J, et al. Neuropeptide-containing neurons of the cerebral cortex are also GABAergic. Proc Natl Acad Sci U S A. 1984; 81(20): 6526–6530, doi: 10.1073/pnas.81.20.6526, indexed in Pubmed: 6149547.
88. Jones EG, Hendry SHC. Co-localization of GABA and neuropeptides in neocortical neurons. Trends Neurosci. 1986; 9: 71–76, doi: 10.1016/0166-2236(86)90026-3.
89. Karagiannis A, Gallopin T, Dávid C, et al. Classification of NPY-expressing neocortical interneurons. J Neurosci. 2009; 29(11): 3642–3659, doi: 10.1523/JNEUROSCI.0058-09.2009, indexed in Pubmed: 19295167.
90. Milner TA, Wiley RG, Kurucz OS, et al. Selective changes in hippocampal neuropeptide Y neurons following removal of the cholinergic septal inputs. J Comp Neurol. 1997; 386(1): 46–59, indexed in Pubmed: 9303524.
91. Marshall CJ, Desroziers E, McLennan T, et al. Defining subpopulations of arcuate nucleus GABA neurons in male, female, and prenatally androgenized female mice. Neuroendocrinology. 2017; 105(2): 157–169, doi: 10.1159/000452105, indexed in Pubmed: 27710963.
92. Haghikia A, Mergia E, Friebe A, et al. Long-term potentiation in the visual cortex requires both nitric oxide receptor guanylyl cyclases. J Neurosci. 2007; 27(4): 818–823, doi: 10.1523/JNEUROSCI.4706-06.2007, indexed in Pubmed: 17251421.
93. Le Roux N, Amar M, Moreau AW, et al. Roles of nitric oxide in the homeostatic control of the excitation-inhibition balance in rat visual cortical networks. Neuroscience. 2009; 163(3): 942–951, doi: 10.1016/j.neuroscience.2009.07.010, indexed in Pubmed: 19591901.
94. Zhang Y, Zhang J, Zhao B. Nitric oxide synthase inhibition prevents neuronal death in the developing visual cortex. Eur J Neurosci. 2004; 20(9): 2251–2259, doi: 10.1111/j.1460-9568.2004.03708.x, indexed in Pubmed: 15525266.
95. O'Gallagher K, Rosentreter RE, Elaine Soriano J, et al. The effect of a neuronal nitric oxide synthase inhibitor on neurovascular regulation in humans. Circ Res. 2022; 131(12): 952–961, doi: 10.1161/CIRCRESAHA.122.321631, indexed in Pubmed: 36349758.

Submitted: 2 February, 2024
Accepted after reviews: 15 March, 2024
Available as AoP: 28 March, 2024